Innovative Method for Controlled Synthesis of Bicomponent Monolayer Films Obtained by Reduction of Diazonium

Julien Billon, Anna Omelchuk, Viacheslav Shkirskiy, Tony Breton, Sylvie Dabos-Seignon, Olivier Alévêque, Eric Levillain, Christelle Gautier

ARTICLE

Innovative Method for Controlled Synthesis of Bicomponent Monolayer Films Obtained by Reduction of Diazonium

Julien Billon,[a] Anna Omelchuk,[a] Viacheslav Shkirskiy,[a†] Sylvie Dabos-Seignon, Olivier Alévêque,[a] Eric Levillain,[a] Tony Breton[a] and Christelle Gautier*[a]

This study presents a novel method based on the electrochemical co-reduction of two aryldiazonium salts, enabling the synthesis of controlled two-component monolayer thin films on carbon in a single step. By introducing a 12-carbon alkyl chain as a spacer between the aryldiazonium function and the functional group, precise control over film thickness and composition was achieved. The alkyl chain effectively standardizes the reduction potentials, enabling the equalization of reactivity and precise stoichiometric control. Experimental results from spectroscopic, electrochemical, and X-ray photoelectron spectroscopy analyses validate the effectiveness of the method in controlling the composition of the mixed layers.

Introduction

The majority of examples involving the functionalization of electrodes using diazonium salts focuses on the reduction of a single type of cation. Nevertheless, for specific applications, it becomes crucial to master the fabrication of bi-functional nanomaterials where one functionality complements the other.[1,2]

However, if no specific precaution is taken, the reduction of two different diazonium salts on an electrode leads to the formation of an organic deposit which is for sure robust, but not necessarily controlled, either in terms of thickness or composition.[3]

To overcome the disadvantages related to the lack of control of the film growth, many alternatives have already been proposed.[4–7] Whether they are based on the degradation of an existing multilayer,[8,9] on the blocking of reactive positions,[10–13] on the lowering of the local concentration of reactive group[14–17] or on the blocking of the electronic transfer through the first layer formed,[18–20] these methods have shown that it is possible to limit the thickness of the films formed to a near-monolayer.

On the other hand, a few rare examples have shown that the composition of bi-component layers can be controlled either by post-functionalizing an electrode previously modified by reduction of a diazonium salt, with a mixture of two reactive entities,[21–24] or by adjusting the composition of a mixture of two diazoniums to be co-reduced.[25–30] The first method mentioned undeniably offers a reliable and effective route for finely varying the proportions of the two immobilized species, but it also has some major drawbacks inherent to the multi-step approach (extensive reaction time and incomplete coupling yields) thus leading to a chemically heterogeneous surface.[31,32] Such major weakness has justified the interest in the second method mentioned (co-reduction) for which the two diazonium salts bearing the function of interest are directly grafted. However, precisely adjusting the concentration ratios of the two precursors in the grafting solution to fine-tune the film composition (even up to 1/10000) proves to be ineffective for certain pairs of diazonium salts. This is due to the fact that the aryl radical production, and thus the grafting kinetics, are influenced by the reduction potential of the precursors, resulting in the predominant attachment of the more easily reducible diazonium on the surface.[25,26,28,33–37]

In this study, we present a novel method for simultaneous co-reduction of two diazonium salts, providing control over film thickness and precise modulation of the organic layer's composition. To achieve stoichiometric grafting and monolayer formation, we introduce a modification to the structure of the diazonium cations, incorporating a 12-carbon alkyl chain between the aromatic ring and the functional group. This structural modification offers two significant advantages. Firstly, as demonstrated in previous studies,[19,20] the 12-carbon alkyl chain restricts electron tunneling through the organic layer, resulting in the growth limitation to a monolayer. Secondly, the alkyl chain acts as a barrier, nullifying the electronic effect of the functional group. This standardization of the diazonium design aims to equalize the reduction potential, promote uniform reactivity of the radicals, and enable precise control over the stoichiometry of the system.

Results and discussion

[a] *Univ Angers, CNRS, MOLTECH-Anjou, SFR MATRIX, F-49000 Angers, France*
† Current address: ITODYS Laboratory, Université Paris Cité, France

Electronic Supplementary Information (ESI) available: Synthesis and characterization of the $aC_{12}Br$ compound; Current versus scan rate recorded on $C_{12}PDI$ monolayers; Spectroscopic response recorded on $aC_{12}PDI$ in solution and on monolayers formed by diazonium reduction on gold. See DOI: 10.1039/x0xx00000x

To reach our goals, two aniline derivatives, each containing a 12-carbon alkyl chain, were synthesized (Scheme 1). The synthesis procedure for obtaining $aC_{12}PDI$ was described in reference,[19] and the synthesis of $aC_{12}Br$ is detailed in Supporting Information (see SI-1).

The choice of functional groups for the two target molecules was guided by the electroactivity and high absorption coefficient of the tetrachloroperylenediimide moiety (PDI, $\varepsilon \approx 50\,000$ L.mol^{-1}.cm^{-1}),[38,39] as well as the presence of halogen atoms on each entity to be immobilized. These factors allow a multimodal characterization of the resulting mixed films through cyclic voltammetry, UV-visible absorption spectroscopy, and X-ray photoelectron spectroscopy (XPS).

A study conducted on $dC_{12}PDI$ (diazonium derivative obtained from $aC_{12}PDI$) revealed the formation of monolayers (with a surface coverage of $\Gamma = 2.5\ 10^{-10}$ mol.cm^{-2}) when the potential used to reduce the molecule is within the range where only the diazonium is reduced i.e. between 0.2 V and -0.3 V versus $Ag/AgNO_3$.[19] To validate the formation of monolayers from $dC_{12}PDI$ and $dC_{12}Br$ compounds, atomic force microscopy (AFM) scratching measurements were performed on carbon pyrolyzed photoresist films (PPF, characterized by low surface roughness < 0.5 nm) to determine the thickness of the obtained layers (AFM images and depth profiles shown in Figures SI-2). The average film thicknesses (estimated from the whole scratched area to have an optimal statistic) as well as the calculated heights of the considered molecules (obtained by molecular mechanics MM2 calculations) are summarized in Table 1.

Table 1. Average film thicknesses determined by AFM scratching measurements and corresponding calculated heights of the considered layer precursors.

Diazonium mixture	Experimental thickness (nm)	Calculated height (nm)
$dC_{12}PDI$ 100%	3.1 ± 0.2	3.14
$dC_{12}Br$ 100%	2.3 ± 0.3	2.27
$dC_{12}PDI/dC_{12}Br$ 50/50	2.6 ± 0.2	-

Film thicknesses values are consistent with the calculated height of $C_{12}PDI$ and $C_{12}Br$ groups, confirming that the films growth is restricted to ultrathin layers.

It remains now to validate the second aspect which involves considering the long chain as a method to regulate the composition of bi-component layers by standardizing the reduction potentials of diazonium. To assess the impact of the alkyl chain on the reduction potential of $dC_{12}PDI$ and $dC_{12}Br$, respectively obtained by in situ diazotization of $aC_{12}PDI$ and $aC_{12}Br$, cyclic voltammograms (CVs) were separately recorded for each cation (Figure 1).

Figure 1 illustrates the irreversible reduction of $dC_{12}PDI$ and $dC_{12}Br$ diazonium salts into the corresponding aryl radicals at potentials of 0.04 V and -0.01 V vs. $Ag/AgNO_3$, respectively. The slight 50 mV difference between these potentials highlights the advantageous role of the alkyl chain, which effectively shields the electronic effects of the functional groups located at its terminal end, enabling a standardization of the aryldiazonium

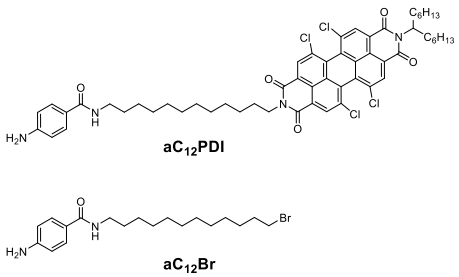

Scheme 1. Structure of the aniline derivatives used for the in-situ formation of diazonium salts.

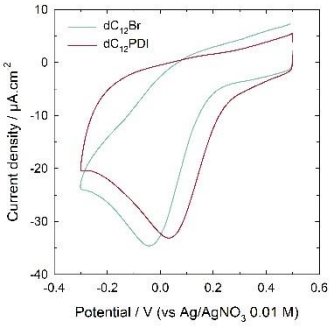

Figure 1. CVs recorded at a scan rate of 50 mV.s^{-1} on a GC electrode, in a solution containing 10^{-3} M aniline derivative ($aC_{12}PDI$ or $aC_{12}Br$) + 5 equiv. of tBuONO and 0.1 M nBu_4NPF_6/DCM.

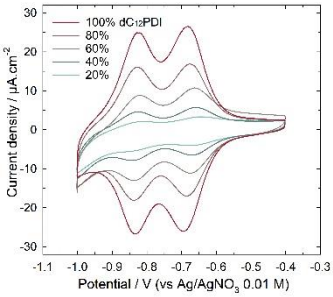

Figure 2: CVs recorded at 100 mV.s^{-1} for mixed $C_{12}PDI/C_{12}Br$-based layers obtained by reduction at 0 V for 5 min in a solution containing $dC_{12}PDI/dC_{12}Br$ molar ratios of 100/0, 80/20, 60/40, 40/60, 20/80. The electrolyte used was 0.1 M nBu_4NPF_6 in DCM and the total concentration of ($dC_{12}PDI$ + $dC_{12}Br$) was 10^{-3} M.

reduction potentials. Thanks to this effect, it becomes possible to simultaneously reduce $dC_{12}PDI$ and $dC_{12}Br$ by applying a potential of 0 V to an electrode immersed in a mixture of the compounds. A series of chronoamperometry experiments was performed using different mixtures of the $dC_{12}PDI/dC_{12}Br$ binary by varying their proportions (100/0, 80/20, 60/40, 40/60, 20/80) and maintaining a total diazonium concentration of [$dC_{12}PDI$] + [$dC_{12}Br$] = 10^{-3} M. The resulting layers were subsequently characterized using cyclic voltammetry, as depicted in Figure 2.

The CVs recorded on various mixed films based on $C_{12}PDI/C_{12}Br$ exhibit two reversible one-electron processes at -0.68 V and -0.82 V, corresponding to the formation of the anion radical $PDI^{\bullet -}$ and the dianion PDI^{2-}, respectively. The minimal peak-to-peak deviation and the linear relationship between current and

scan rate confirmed the confinement of these species on the film surface (see Figure SI-3).

As expected, a decrease in the proportion of PDI units in the grafting solution leads to a decrease in the intensity of the characteristic peaks associated with immobilized PDI. Consequently, as the diazonium mixture becomes depleted in PDI, the surface concentration of PDI (Γ_{PDI}), determined by integration of the CV, decreases. For instance, from a value of 2.3 10^{-10} mol.cm^{-2} for a layer composed of 100% PDI, the surface concentration is lowered to 0.3 10^{-10} mol.cm^{-2} when the diazonium mixture contains 20% PDI.

To examine the correlation between the quantity of immobilized PDI and the PDI content in the grafting solution, the surface concentration of PDI was plotted as a function of the molar percentage of PDI in the deposition solution (Figure 3, black markers).

Figure 3 illustrates a strong correlation between the proportions of the species in the grafting mixtures ($aC_{12}PDI/aC_{12}Br$) and their proportions in the immobilized state since an almost linear increase of Γ_{PDI} is obtained with increasing concentration of $dC_{12}PDI$ in the diazonium mixture. Importantly, a similar trend was observed when longer grafting times (30 min) were employed to form the mixed layers (Figure 3, red markers). This finding shows that extending the grafting process beyond 5 minutes does not provide additional benefits and consequently that the process is self-limited within a short time.

To leverage the absorption properties of the chromophore in the visible range, spectroelectrochemical (SEC) experiments were conducted on $C_{12}PDI/C_{12}Br$ films (Figure 4).

Upon reduction, the immobilized PDI exhibits a negative relative absorption, which corresponds to the optical signature of PDI across a wide wavelength range (520-780 nm). The absorption minimum is observed at 545 nm. The formation of the $PDI^{\bullet -}$ radical species gives rise to absorption bands around 480 nm and 800 nm, while the formation of the PDI^{2-} dianion results in an absorption peak at approximately 720 nm. Although the signal intensity is lower in a mixed layer containing 40% PDI compared to a layer composed solely of PDI, the characteristic bands exhibit similar properties, indicating that the structure of immobilized chromophores is not influenced by the surrounding species.

Figure 5A presents the 2D sections (i.e. ΔAbs vs. wavelength) extracted through principal component analysis at t = 60 s, which corresponds to the absorption maximum observed during PDI^{2-} formation. These sections are used to compare the SEC responses of $C_{12}PDI$ layers, ranging from 100% to 20% dilutions.

Upon initial observation, the 2D sections appear to be similar regardless of the PDI surface concentration. However, it is important to note that they differ from those observed for $aC_{12}PDI$ molecule in solution (refer to Figure SI-4A),[38] as well as those observed on gold surfaces, including self-assembled monolayers[38,39] and monolayers formed by diazonium reduction (Figure SI-4B). These distinctions will be the subject of further investigation.

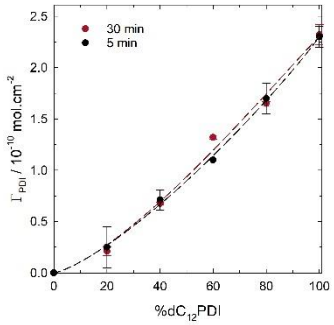

Figure 3. Surface coverages of PDI determined from the integration of CVs shown in Figure 2 vs the percentage of $dC_{12}PDI$ in the grafting solution. The black markers represent the surface coverages obtained by reduction at 0 V for 5 min, while the red markers represent the surface coverages obtained by reduction at 0 V for 30 min.

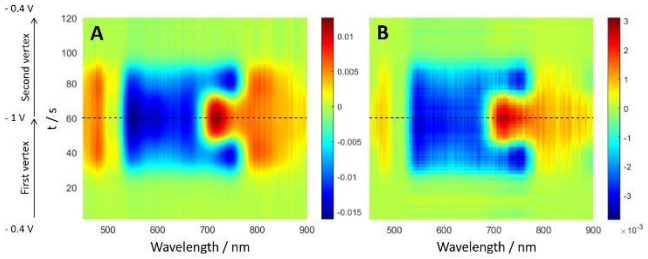

Figure 4. A. Time-dependent variation of the optical response recorded during cyclic voltammetry recorded at 10 mV.s^{-1} (in nBu_4NPF_6 0.1 M/DCM) on a GC electrode modified with a $C_{12}PDI$ monolayer. The surface concentration of the $C_{12}PDI$ monolayer deposited by chronoamperometry at -0 V for 5 min in a solution of $dC_{12}PDI$ 10^{-3} M, nBu_4NPF_6 0.1 M/DCM is 2.3 × 10^{-10} mol.cm^{-2}. B. Similar analysis performed on a GC electrode modified with $dC_{12}PDI$ and $dC_{12}Br$, where the concentrations of $dC_{12}PDI$ and $dC_{12}Br$ were 0.4 × 10^{-3} M and 0.6 × 10^{-3} M, respectively. The resulting layer was characterized by a PDI surface concentration of 0.8 × 10^{-10} mol.cm^{-2}.

The absorbance correlates with the quantity of immobilized PDI species, as the charge determined by cyclic voltammetry does. Hence, it was interesting to examine the evolution of ΔAbs in relation to the percentage of $dC_{12}PDI$ in solution. In this regard, the absorption maximum corresponding to the disappearance of the neutral PDI species at 545 nm was plotted as a function of the percentage of $dC_{12}PDI$ in the solution (Figure 5B), showing a good agreement with the results obtained by cyclic voltammetry. Despite the broadened bands, the behavior exhibits close to linear characteristics.

Consequently, based on the spectroscopic and electrochemical data, precise control over the PDI surface concentration can be achieved simply by adjusting the diazonium concentration.

However, these experiments, which focus on PDI quantification, do not provide insight into the amount of immobilized $C_{12}Br$ on the surface, as only PDI can be quantified through spectroelectrochemistry. To quantify both $C_{12}PDI$ and $C_{12}Br$ (thanks to the respective presence of chlorine and bromine atoms), XPS experiments were conducted on mixed layers prepared on GC plates under the same conditions as described above. Figure 6 displays the Cl2p and Br3d core level spectra recorded on the mixed organic films obtained from $dC_{12}PDI/dC_{12}Br$ mixtures at various proportions.

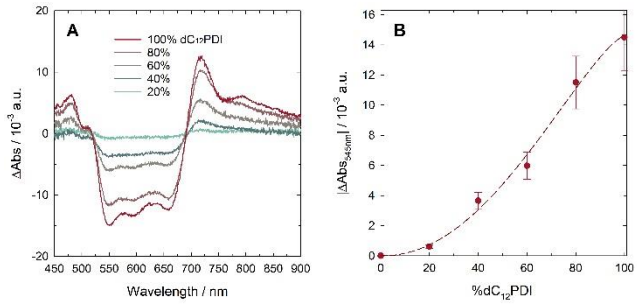

Figure 5. A. 2D sections extracted from SEC experiments performed at {-1 V; t = 60 s} on GC electrodes modified with $dC_{12}PDI$ and $dC_{12}Br$. The total concentration of $dC_{12}PDI$ and $dC_{12}Br$ was 10^{-3} M and the electrodes were reduced at 0 V for 5 min. B. Absorbance maximum at 545 nm as a function of the percentage of $dC_{12}PDI$ in the grafting solution.

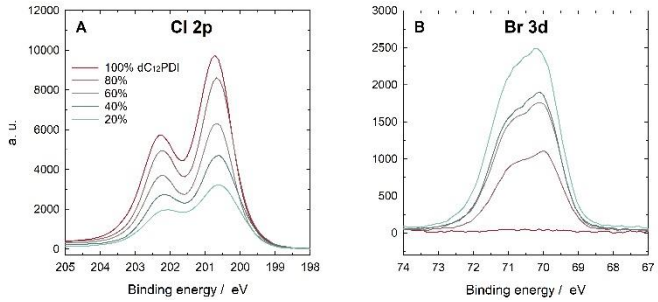

Figure 6. XPS core-level spectra recorded on GC plates functionalized by reduction at 0 V during 5 min in mixtures containing $dC_{12}PDI/dC_{12}Br$ molar ratios of 100/0, 80/20, 60/40, 40/60, 20/80, where the total concentration of $dC_{12}PDI+dC_{12}Br$ was 10^{-3} M in 0.1 M nBu_4NPF_6/DCM. (A) Cl 2p core-level spectrum, (B) Br 3d core-level spectrum.

Figure 6A shows an increase in chlorine content as the PDI concentration in the grafting solution increases. Similarly, Figure 6B reveals an increase in the Br3d component with increasing concentrations of $dC_{12}Br$.

To calculate the percentage of PDI on the modified surface, peak fitting and integration were performed on the spectra using CASA XPS software (fitting curves shown in Figure SI-5). Equation (1) was employed for this calculation. The resulting values were then plotted as a function of the percentage of PDI in the solution (Figure 7, green markers).

$$\%PDI\ surf = \frac{\frac{\%Cl}{4}}{\frac{\%Cl}{4}+\%Br} \quad (1)$$

For each layer, the PDI/Br ratio on the modified surface shows a close resemblance to the ratio present in the initial diazonium mixture. In order to facilitate comparison, the graph incorporates values obtained from electrochemical and spectroscopic data, assuming $\Gamma 100\%(C_{12}PDI) = \Gamma 100\%(C_{12}Br)$. The percentages of PDI on the surface calculated from these data correspond to a normalized number with respect to a surface prepared with 100% $C_{12}PDI$ in solution. The remarkable agreement among the results obtained from the three methods serves as confirmation of the effective control over the composition of the two-component layers.

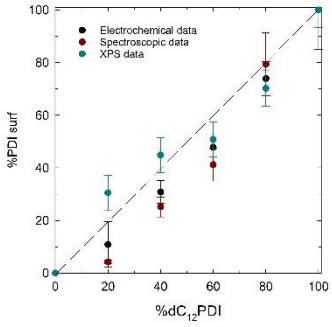

Figure 7. Percentage of PDI on the surface, indicated by green markers (calculated from XPS data), black markers (calculated from electrochemical data) and red markers (calculated from spectroscopic data), plotted as a function of the percentage of $dC_{12}PDI$ in the grafting solution.

Conclusions

This study introduces a novel method for the simultaneous control of thickness and composition in two-component layers obtained through the co-reduction of aryldiazonium salts. By incorporating a 12-carbon alkyl chain as a spacer, the film thickness is effectively controlled, and the composition of the mixed layers is precisely regulated. The results obtained from AFM, spectroscopic, electrochemical and XPS analyses confirm the ability to control the surface concentrations of the immobilized species, demonstrating the reliability and accuracy of the method.

This one-step approach offers a promising route for the fabrication of stable and reproducible bi-functional nanomaterials with tailored properties. Further investigations into the structural and electronic properties of the functional layers will contribute to pave the way for future advancements in this field.

Experimental

Materials and Reagents

The $aC_{12}Br$ compound was synthesized by a three-step procedure described in detail in SI-1 in Supporting Information. The final product $aC_{12}Br$ was used for in situ generation of diazonium salts, further called $dC_{12}Br$. Tetrabutylammonium hexafluorophosphate (nBu_4NPF_6, Sigma-Aldrich), CH_2Cl_2 (HPLC grade, VWR chemicals), and tert-butyl nitrite (tBuONO, Sigma-Aldrich) were used as received. Milli-Q water (18 MΩ.cm) was used during polishing and for rinsing the electrodes. A disk glassy carbon (GC) electrode was supplied by Bioanalytical Systems Inc. (Model MF-2012 with a geometric area of 0.07 cm^2).

Electrochemical Grafting

Prior to each experiment, the GC working electrode underwent a series of preparation steps. It was polished with a 0.04 µm Al_2O_3 slurry (PRESI) and then subjected to sonication in water, acetonitrile, and dichloromethane (DCM) for 2 minutes. The electrode was then rinsed with DCM. Electrochemical experiments were conducted using a BioLogic potentiostat (VSP

model with four channels). Electrochemical grafting was performed in a three-electrode cell containing 2 mL of a 0.1 M nBu_4NPF_6 solution in DCM, with a concentration of 10^{-3} M of the mixture ($aC_{12}PDI+aC_{12}Br$). Prior to grafting, 5 equivalents of tBuONO were added to the solutions and stirred for 10 minutes. The grafting potential was then applied to generate aryl radicals from in situ generated diazoniums, following the procedure described in previous literature.[19,20] The counter electrode used was a platinum (Pt) rod, and the reference electrode was $Ag/AgNO_3$ (0.01 M in 0.1 M nBu_4NPF_6 in acetonitrile). After deposition of the organic layers, the GC electrodes were sonicated for 2 minutes and washed with DCM. The surface coverage of PDI groups was estimated by analyzing cyclic voltammograms obtained in a 0.1 M nBu_4NPF_6/DCM solution. The surface coverage (Γ) was calculated using the formula $\Gamma = Q/nFS$, where Q is the charge estimated by integrating the reduction peaks on the cyclic voltammogram, n = 2 is the number of electrons involved, F = 96485 $C.mol^{-1}$ is the Faraday constant, and S = 0.07 cm^2 is the surface area of the electrode. All experiments were performed at room temperature, approximately 293 K.

Atomic Force Microscopy (AFM) scratching measurements

The thickness measurements were carried out using the AFM scratching method,[40] with a NanoObserver Microscope from CSInstruments. The acquired images were processed using the free and open source software Gwyddion.[41] Thickness values were calculated from the average profile extracted from the AFM images.

Spectroelectrochemical (SEC) Characterization

Spectroelectrochemical measurements were conducted in reflection mode using a custom-built bench setup inspired by a previously reported high-resolution bench.[42,43] The setup comprises spectrometric modules (Flame CCD spectrometer from Ocean Optics and SL1 tungsten/halogen light source from StellarNet) coupled to a BioLogic SP-150 potentiostat. The experimental setup involved a home-designed Teflon three-electrode cell with a GC working electrode, a platinum (Pt) counter electrode, and an $Ag/AgNO_3$ reference electrode (0.01 M in 0.1 M nBu_4NPF_6 in acetonitrile), which was identical to the electrochemical grafting setup. The connection between the light source, the electrochemical cell, and the spectrophotometer was established using a "Y-shaped" optical fiber bundle from IDIL Fibres Optiques. This bundle comprised 18 fibers to guide the light to the cell and 19 fibers to collect the reflected light from the cell, directing it to the CCD detector. The spectrophotometer had a spectral range of 320-1080 nm, a spectral resolution close to 0.5 nm, and an acquisition bandwidth of 2 MHz. The acquisition rate of the spectrometer was set to 10 frames per second (integration time of 100 ms), which corresponded to 1 frame per mV at a scan rate of 10 $mV.s^{-1}$. The EC-Lab software controlled the BioLogic potentiostat and triggered the acquisition of spectral data, ensuring synchronized time scales between the electrochemical and spectroscopic measurements. Custom MATLAB software was developed in-house for data plotting and processing. In each data set, the reference intensity (Iref) was determined by averaging the intensity of the first 10 measured frames in which no change in the redox state of the studied species was observed. As a result, the variation in absorbance (ΔAbs) was monitored rather than the absolute absorbance values (Abs).

X-ray photoelectron spectroscopy (XPS) Experiments

XPS data were acquired using a Kratos Axis Ultra spectrometer. The X-ray source employed was monochromated Al Kα source operating at 1486.6 eV. Spectra were collected at a take-off angle of 90°, using a spot size of 0.7 × 0.3 mm^2 at a pressure below 10^{-8} mbar. High-resolution scans were performed with a step size of 0.1 eV and a pass energy of 40 eV. Calibration was done using C1s as a reference, with a binding energy of 284.5 eV, without the need for an internal standard. XPS spectra were analyzed using the curve-fitting software CASA XPS. The background subtraction was performed using the U2 Tougaard method, followed by fitting the peaks using a pseudo-Voigt function that combined Gaussian and Lorentzian functions.

Author Contributions

The manuscript was written through contributions of all authors. All authors have given approval to the final version of the manuscript.

Conflicts of interest

There are no conflicts to declare.

Acknowledgements

The authors thank MATRIX SFR of the University of Angers and more precisely the ASTRAL and CARMA platforms for the characterization of organic compounds. They are grateful to Jonathan Hamon and Vincent Fernandez from the “Institut des Matériaux de Nantes Jean Rouxel” for their assistance in XPS measurements. J.B. thanks the University of Angers for a PhD fellowship and V.S. acknowledges the LUMOMAT funding program for a postdoctoral fellowship.

References

1 J. J. Gooding, *Electroanalysis*, 2008, **20**, 573–582.
2 C. Jiang, S. Moraes Silva, S. Fan, Y. Wu, M. T. Alam, G. Liu and J. Justin Gooding, *J. Electroanal. Chem.*, 2017, **785**, 265–278.
3 D. Belanger and J. Pinson, *Chem. Soc. Rev.*, 2011, **40**, 3995–4048.
4 T. Breton and A. J. Downard, *Aust. J. Chem.*, 2017, **70**, 960.
5 P. Hapiot, C. Lagrost and Y. R. Leroux, *Curr. Opin. Electrochem.*, 2018, **7**, 103–108.
6 J. Pinson and F. I. Podvorica, *Curr. Opin. Electrochem.*, 2020, **24**, 44–48.
7 T. Breton and C. Gautier, in *Aryl Diazonium Salts and Related Compounds: Surface Chemistry and Applications*, eds. M. M. Chehimi, J. Pinson and F. Mousli, Springer International Publishing, Cham, 2022, pp. 97–120.

8 L. T. Nielsen, K. H. Vase, M. Dong, F. Besenbacher, S. U. Pedersen and K. Daasbjerg, *J. Am. Chem. Soc.*, 2007, **129**, 1888–1889.
9 K. Malmos, M. Dong, S. Pillai, P. Kingshott, F. Besenbacher, S. U. Pedersen and K. Daasbjerg, *J. Am. Chem. Soc.*, 2009, **131**, 4928–4936.
10 C. Combellas, F. Kanoufi, J. Pinson and F. I. Podvorica, *J. Am. Chem. Soc.*, 2008, **130**, 8576–8577.
11 Y. R. Leroux, H. Fei, J.-M. Noël, C. Roux and P. Hapiot, *J. Am. Chem. Soc.*, 2010, **132**, 14039–14041.
12 A. Mattiuzzi, I. Jabin, C. Mangeney, C. Roux, O. Reinaud, L. Santos, J.-F. Bergamini, P. Hapiot and C. Lagrost, *Nat. Commun.*, 2012, **3**, 1130.
13 V. Q. Nguyen, X. Sun, F. Lafolet, J.-F. Audibert, F. Miomandre, G. Lemercier, F. Loiseau and J.-C. Lacroix, *J. Am. Chem. Soc.*, 2016, **138**, 9381–9384.
14 J. Ghilane, P. Martin, O. Fontaine, J.-C. Lacroix and H. Randriamahazaka, *Electrochem. Commun.*, 2008, **10**, 1060–1063.
15 M. Kongsfelt, J. Vinther, K. Malmos, M. Ceccato, K. Torbensen, C. S. Knudsen, K. V. Gothelf, S. U. Pedersen and K. Daasbjerg, *J. Am. Chem. Soc.*, 2011, **133**, 3788–3791.
16 I. López, M. Cesbron, E. Levillain and T. Breton, *ChemElectroChem*, 2018, **5**, 1197–1202.
17 L. Pichereau, I. López, M. Cesbron, S. Dabos-Seignon, C. Gautier and T. Breton, *Chem. Commun.*, 2019, **55**, 455–457.
18 M. Tanaka, T. Sawaguchi, Y. Sato, K. Yoshioka and O. Niwa, *Langmuir*, 2011, **27**, 170–178.
19 V. Shkirskiy, J. Billon, E. Levillain and C. Gautier, *Langmuir*, 2021, **37**, 12834–12841.
20 J. Billon, V. Shkirskiy, S. Dabos-Seignon, T. Breton and C. Gautier, *Phys. Chem. Chem. Phys.*, 2022, **24**, 14294–14298.
21 G. Tuci, C. Vinattieri, L. Luconi, M. Ceppatelli, S. Cicchi, A. Brandi, J. Filippi, M. Melucci and G. Giambastiani, *Chem. – Eur. J.*, 2012, **18**, 8454–8463.
22 G. Tuci, D. Mosconi, A. Rossin, L. Luconi, S. Agnoli, M. Righetto, C. Pham-Huu, H. Ba, S. Cicchi, G. Granozzi and G. Giambastiani, *Chem. Mater.*, 2018, **30**, 8257–8269.
23 M. Cesbron, E. Levillain, T. Breton and C. Gautier, *ACS Appl. Mater. Interfaces*, 2018, **10**, 37779–37782.
24 M. Cesbron, S. Dabos-Seignon, C. Gautier and T. Breton, *Electrochimica Acta*, 2020, **345**, 136190.
25 L. V. Hai, S. Reisberg, A. Chevillot-Biraud, V. Noel, M. C. Pham and B. Piro, *Electrochimica Acta*, 2014, **140**, 49–58.
26 C. Jiang, M. T. Alam, S. M. Silva, S. Taufik, S. Fan and J. J. Gooding, *ACS Sens.*, 2016, **1**, 1432–1438.
27 L. Zhang, N. Vilà, A. Walcarius and M. Etienne, *ChemElectroChem*, 2018, **5**, 2208–2217.
28 S. C. Binding, I. Pernik, V. R. Gonçales, C. M. Wong, R. F. Webster, S. Cheong, R. D. Tilley, A. E. Garcia-Bennett, J. J. Gooding and B. A. Messerle, *Organometallics*, 2019, **38**, 780–787.
29 L. Santos, A. Mattiuzzi, I. Jabin, N. Vandencasteele, F. Reniers, O. Reinaud, P. Hapiot, S. Lhenry, Y. Leroux and C. Lagrost, *J. Phys. Chem. C*, 2014, **118**, 15919–15928.
30 H. Valkenier, V. Malytskyi, P. Blond, M. Retout, A. Mattiuzzi, J. Goole, V. Raussens, I. Jabin and G. Bruylants, *Langmuir*, 2017, **33**, 8253–8259.
31 C. Gautier, I. López and T. Breton, *Mater. Adv.*, 2021, **2**, 2773–2810.
32 T. Wu, C. M. Fitchett, P. A. Brooksby and A. J. Downard, *ACS Appl. Mater. Interfaces*, 2021, **13**, 11545–11570.
33 C. Jiang, M. T. Alam, S. G. Parker, N. Darwish and J. J. Gooding, *Langmuir*, 2016, **32**, 2509–2517.
34 C. Louault, M. D'Amours and D. Bélanger, *ChemPhysChem*, 2008, **9**, 1164–1170.
35 G. Liu, M. Chockalingham, S. M. Khor, A. L. Gui and J. J. Gooding, *Electroanalysis*, 2010, **22**, 918–926.
36 S. M. Khor, G. Liu, C. Fairman, S. G. Iyengar and J. J. Gooding, *Biosens. Bioelectron.*, 2011, **26**, 2038–2044.
37 C. Esnault, N. Delorme, G. Louarn and J.-F. Pilard, *ChemPhysChem*, 2013, **14**, 1793–1796.
38 S. Bkhach, Y. Le Duc, O. Alévêque, C. Gautier, P. Hudhomme and E. Levillain, *ChemElectroChem*, 2016, **3**, 887–891.
39 S. Bkhach, O. Alévêque, Y. Morille, T. Breton, P. Hudhomme, C. Gautier and E. Levillain, *ChemElectroChem*, 2017, **4**, 601–606.
40 P. A. Brooksby and A. J. Downard, *Langmuir*, 2004, **20**, 5038–5045.
41 D. Nečas and P. Klapetek, *Open Phys.*, 2012, **10**, 181–188.
42 O. Alévêque, E. Levillain and L. Sanguinet, *Electrochem. Commun.*, 2015, **51**, 108–112.
43 O. Alévêque, C. Gautier and E. Levillain, *Curr. Opin. Electrochem.*, 2019, **15**, 34–41.
…